Electronic Supplementary Material (ESI) for Journal of Materials Chemistry A.

Supporting Information

Tuning the Separation Properties of Zeolitic Imidazolate Framework Core-Shell Structures via Post-Synthetic Modification

Javier Sánchez-Laínez[1], Adrián Veiga[1], Beatriz Zornoza[1], Salvador R.G. Balestra[2], Said Hamad[2], A. Rabdel Ruiz-Salvador[2], Sofia Calero[2], Carlos Téllez[1] and Joaquín Coronas[1]**

[1] J. Sánchez-Laínez, Dr. B. Zornoza, Prof. Dr. C. Téllez, Prof. Dr. J. Coronas
Instituto de Nanociencia de Aragon (INA) and Chemical Engineering and Environmental Department
Universidad de Zaragoza
C/ Mariano Esquillor, s/n., 50018 Zaragoza (Spain)
E-mail: bzornoza@unizar.es, coronas@unizar.es

[2] S. R.G. Balestra, Dr. S. Hamad, Dr. A. R. Ruiz-Salvador, Prof. Dr. S. Calero
Department of Physical, Chemical and Natural Systems
Univ. Pablo de Olavide
Ctra. de Utrera km. 1, 41013 Seville (Spain)

*Corresponding authors

Study of the post-synthetic modification reaction at different temperatures and bIm concentrations:

Table S1. bIm amount in the reaction medium, reaction temperature and reaction time in the post-synthetic modification reactions of ZIF-8 and the resulting ZIF.

bIm concentration	6.5 g/L	6.5 g/L	13 g/L	26 g/L	26 g/L
ZIF-8 concentration	3.3 g/L	3.3 g/L	3.3 g/L	3.3 g/L	3.3 g/L
Temperature	30 ^{0}C	65 ^{0}C	30 ^{0}C	90 ^{0}C	90 ^{0}C
Time	7 days	3 days	3 days	1 day	3 days
Resulting ZIF	ZIF-7/8 hybrid (10 %mol bIm)	ZIF-7/8 hybrid (10 %mol bIm)	ZIF-7/8 hybrid (10 %mol bIm)	ZIF-7(II)	ZIF-7(I)

Different bIm concentrations and temperatures were tested to study the influence of these variables on the post-synthetic modification reaction of ZIF-8 (see Table S1), providing tunable reaction conditions. As a result, the ZIF-7/8 hybrid (10 %mol bIm) was obtained in 3 days at 65 ^{0}C and with an initial bIm concentration in the reaction medium of 6.5 g/L or at 30 ^{0}C with a bIm concentration of 13 g/L. The same hybrid material was obtained from a reaction at 30 °C during 7 days when the initial bIm concentration was 6.5 g/L.

Reaction modeling:

The post-synthetic modification reaction of ZIF-8 was adjusted using the shrinking core model for spherical particles of unchanging size of Levenspiel. Neglecting the contribution of the gas film resistance, the resulting integrated equation is shown in Eq. S1:

$$t = \frac{\rho_{ZIF-8} \cdot R^2}{6 \cdot b \cdot C_{bIm} \cdot D_e}\left[1 - 3\left(1 - X_{ZIF-8}\right)^{\frac{2}{3}} + 2\left(1 - X_{ZIF-8}\right)\right] + \frac{\rho_{ZIF-8} \cdot R}{b \cdot C_{bIm} \cdot k_s}\left[1 - \left(1 - X_{ZIF-8}\right)^{\frac{1}{3}}\right] \quad [Eq.(S1)]$$

The values and meaning of the different terms of both equations can be seen in Table S1. Both the kinetic constant and the diffusion coefficient were calculated from the slopes resulting from a multiple regression fit of the empirical data recorded in Table S2.

Table S2. Values for the shrinking core model.

ρ_{ZIF-8}	ZIF-8 density	1.3 g/mL
R	Particle radius	124 nm
b	Stoichiometric factor	1
C_{bIm}	bIm concentration	13 g/L
D_e	Diffusion coefficient in the ash film	$2.86 \cdot 10^{-7}$ cm²/s
k_s	Kinetic constant	$1.36 \cdot 10^{-4}$ cm/s

Table S3. Empirical and calculated values of the post-synthetic modification reaction.

Time (h)	Empirical X_{ZIF-8}	Calculated X_{ZIF-8}	% error= $\frac{\lvert X_{empirical} - X_{calculated} \rvert}{X_{empirical}} \cdot 100$
0	0.00	0.00	0.0
0.50	0.05	0.04	16.4
0.75	0.06	0.06	4.5
1	0.07	0.07	2. 8
1.5	0.09	0.08	15.4
3	0.14	0.14	22.7
4.5	0.15	0.18	18.2
5	0.17	0.19	13.7
6	0.22	0.21	3.6
7	0.26	0.23	11.4
18	0.40	0.38	4.9
19	0.42	0.39	7.3
20	0.42	0.40	5.5
26	0.46	0.45	1.4
42	0.58	0.56	4.3
48	0.55	0.59	7.4
72	0.79	0.70	11.5
168	0.98	0.93	5.1

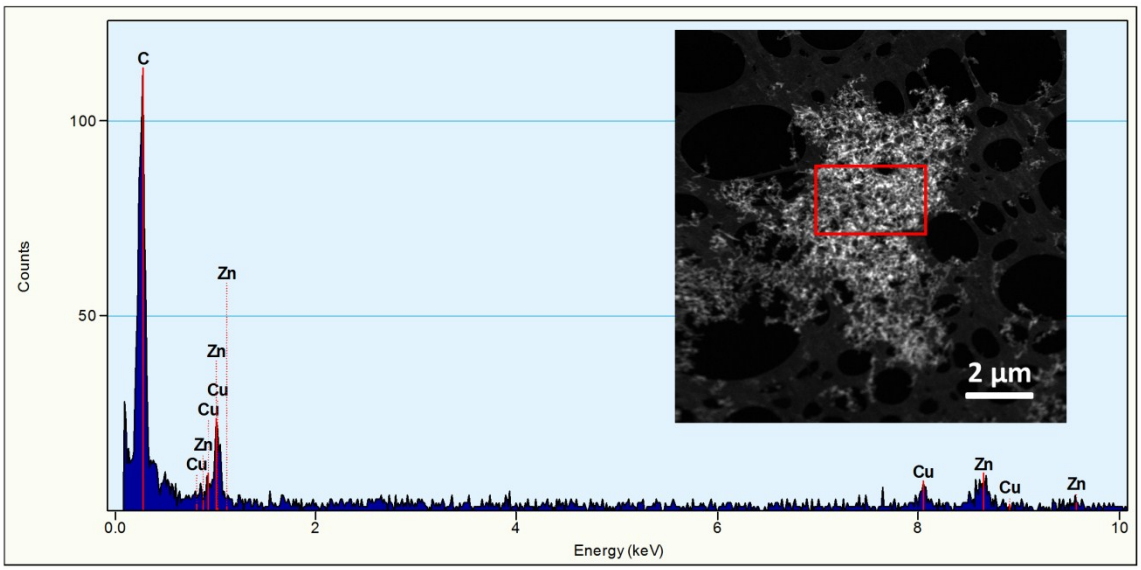

Fig. S1. TEM image and EDX analysis of the reaction medium after the post-synthetic modification reaction.

The reaction medium was evaluated by EDX once the post-synthetic modification had finished and the results are shown in Fig. S1. The dispersion was centrifuged and the supernatant was filtered twice using 0.14 µm filters to remove any remaining solid particles. The solvent was evaporated and replaced by MeOH. One drop of liquid was deposited onto a TEM grid for characterization. An amorphous solid could be found in the sample, where traces of Zn were detected, as well as Cu from the grid. This residual solid may come from part of the original ZIF-8 nanoparticles that was desorbed at the beginning of the post-synthetic modification reaction. This may explain the relative high fitting errors of the kinetic model (Table S3)

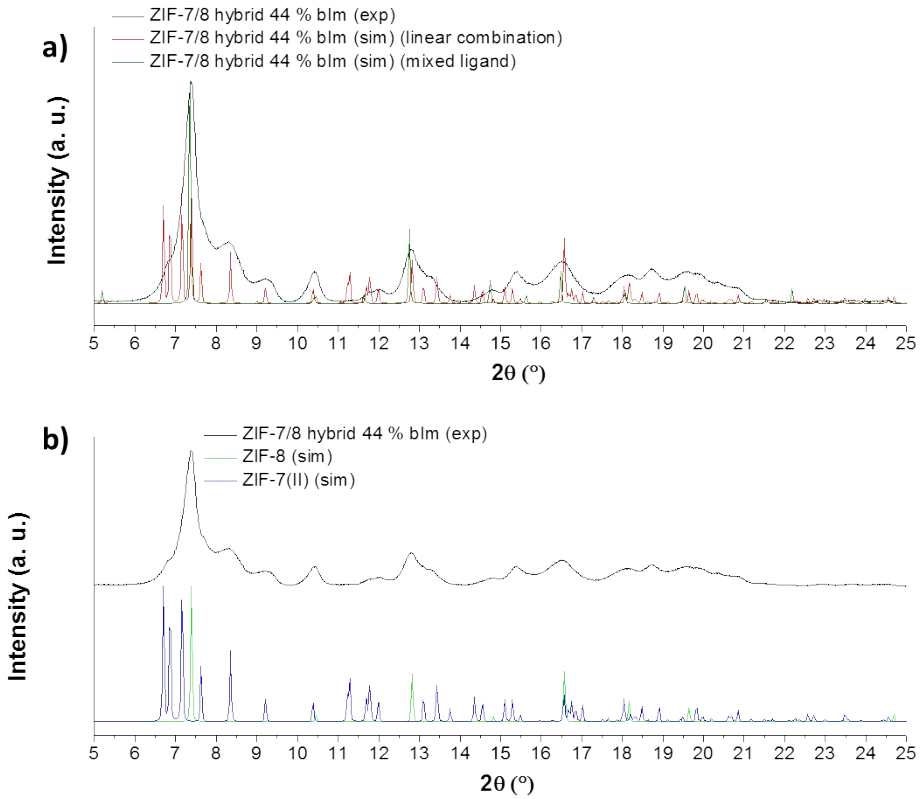

Fig. S2. XRD patterns of ZIF-7/8 hybrid 44% mol bIm, empirical and simulated according to a mixed-ligand structure and a linear combination of ZIF-7 and ZIF-8 (a) and comparison of empirical spectrum with simulated diffractograms of ZIF-8 and ZIF-7(II) from the literature (b).[9]

ZIFs characterization:

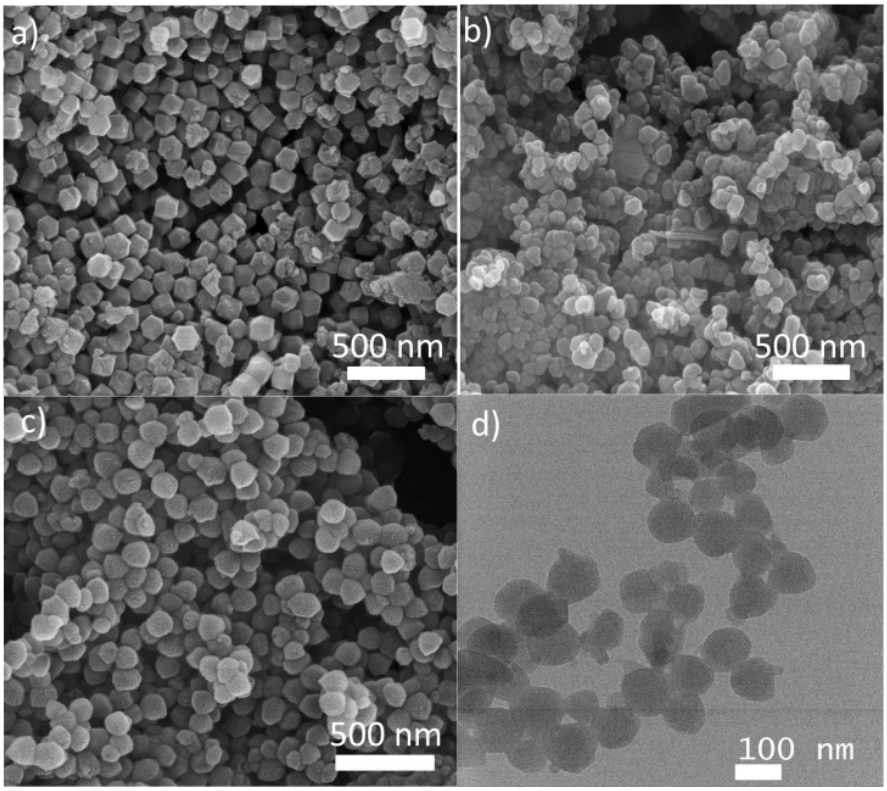

Fig. S3. SEM images of ZIF-8 (a), ZIF-7 (b) and ZIF-7/8 hybrid (c) and TEM image of ZIF-7/8 hybrid (d).

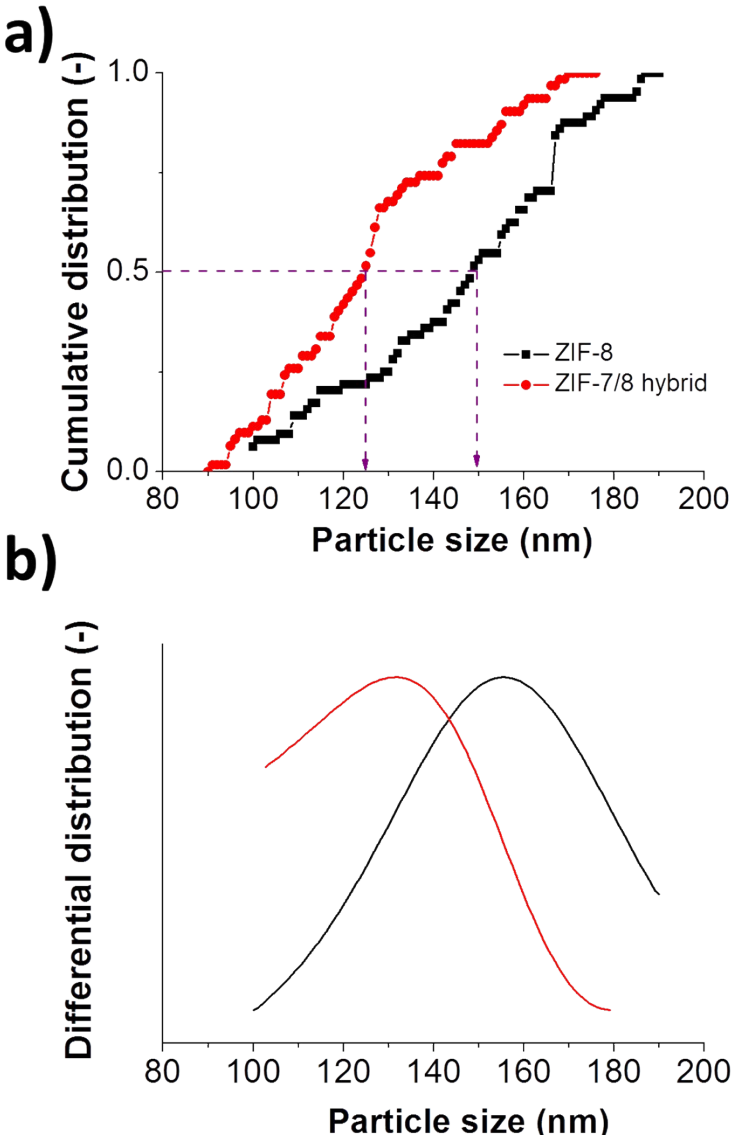

Fig. S4. Cumulative (a) and differential (b) particle size distribution of the ZIF-8 and ZIF-7/8 hybrid nanoparticle samples.

Fig. S4a shows the normalized cumulative number of particles as a function of the particle size. From this plot, average particle sizes for each sample (124 and 150nm) were obtained at $N/N_T = 0.5$, N and N_T being the number and total number of particles, respectively. In addition, the differential distributions were calculated (Fig. S4b), providing predominant particle sizes (modes), whose values are similar to the corresponding averages.

Table S4. EDX analysis of the ZIF-7/8 (hybrid) 10%mol bIm.

Element	Weight	Atomic %	Uncertanty %	Detector correction	k-Factor
C(K)	81.99	88.65	1.50	0.26	4.032
N(K)	10.66	9.89	0.59	0.26	3.903
Zn(K)	7.33	1.45	0.27	0.99	1.686

Table S4 shows the EDX quantification of the hybrid sample shown in Fig. 2. The average atomic N/Zn proportion was 7/1, which is similar to the theoretical 8/1 expected (one atom of Zn for every two imidazole molecules, thus four atoms of N).

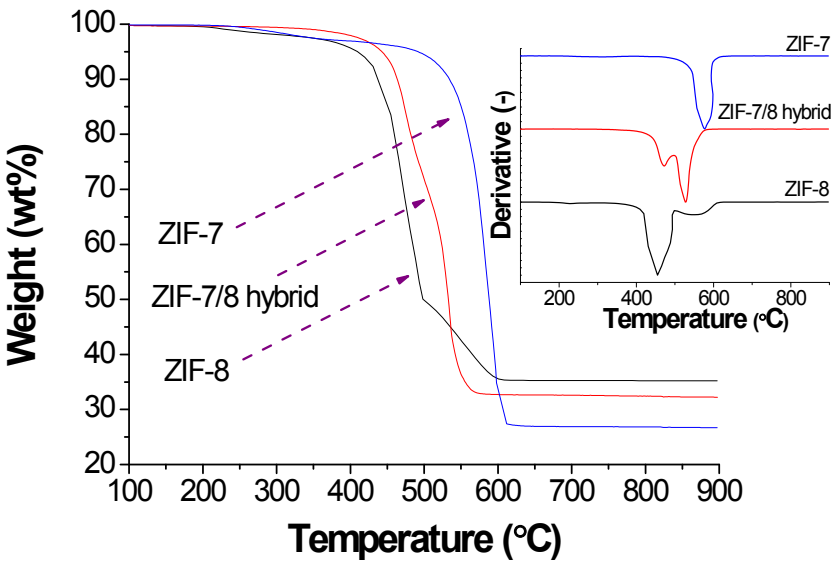

Fig. S5. TGA and derivative (inset) of ZIF-7, ZIF-8 and ZIF-7/8 hybrid in air.

Thermogravimetric analyses (TGA) in air can be seen in Fig. S5. ZIF-8 shows a big weight loss at 455 ^{0}C followed by a small one at 552 ^{0}C related to the decomposition of the mIm contained in its structure. In the case of ZIF-7, it shows a higher onset temperature (576 ^{0}C), due to the greater thermal stability of bIm (ZIF-7 linker). The existence of these two decomposition steps in the hybrid TGA

corresponds to the coexistence of mIm and bIm in the framework structure. The existence of a continuous TGA curve, different to those of the neat ZIFs, instead of two isolated decomposition steps is indicative of the existence of a framework against a physical mixture of ZIF-7 and ZIF-8.

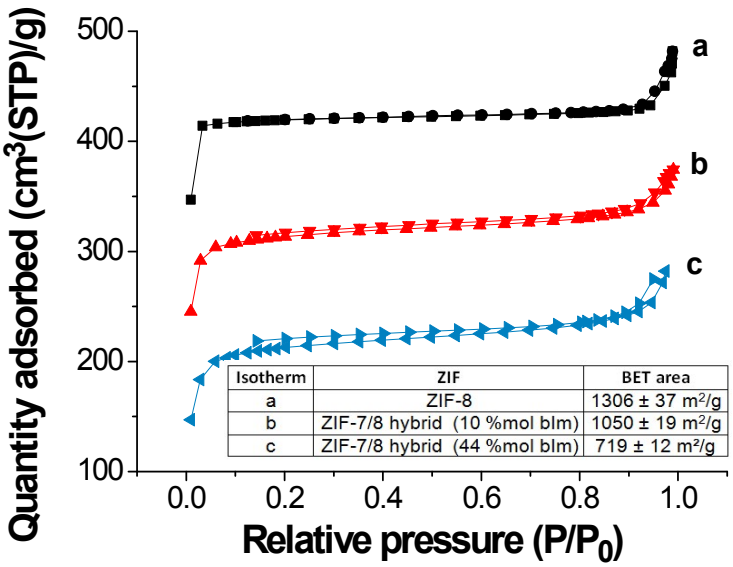

Fig. S6. Empirical N_2 adsorption isotherms of activated ZIF-8 and ZIF-7/8 hybrids at 77 K and calculated BET areas (inset).

N_2 adsorption was measured for ZIF-8 and the ZIF-7/8 hybrids to study their porosity (see Fig. S6) after the corresponding activation with MeOH. The adsorption isotherm of ZIF-7 is not included since this compound was unable to adsorb N_2 at this range of pressures. According to their shape, both isotherms can be classified as Type I, typical of microporous materials. The standard deviation for BET area is that provided by the sorption device.

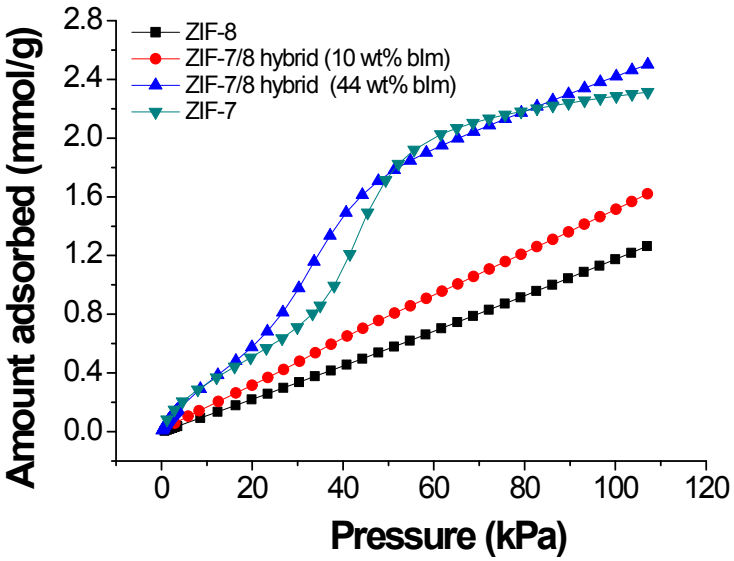

Fig. S7. Empirical CO_2 adsorption isotherms of activated ZIF-8, ZIF-7/8 hybrids and ZIF-7 at 273 K.

CO_2 adsorption was also measured for ZIF-7, ZIF-8 and both hybrids to study their porosity in deep (see Fig. S7). ZIF-8 shows a little CO_2 uptake (1.3 mmol/g at 110 kPa) since the pressure during the experiment is not high enough to open their pores.[10] The isotherm of ZIF-7 shows inflexion points, already reported in the literature.[11, 12] The framework containing a 10% of bIm increases this gas uptake a 20% at the same pressure, while the hybrid containing a 44 % of this linker is able to adsorb as much as bare ZIF-7, thus 2.4 mmol/g of CO_2 at 110 kPa.

Table S5. Heat of adsorption of CO_2 and H_2 in mixing ligands ZIF structures.

Structure (% bIm)	CO_2 Heat of adsorption (kJ/mol)	H_2 Heat of adsorption (kJ/mol)
100 (ZIF-7)	-30.3	-5.9
89	-28.2	-5.3
81	-27.8	-4.9
69	-24.5	-4.5
58	-18.4	-3.8
42	-16.0	-3.3
29	-13.5	-2. 9
21	-13.15	-2.9
8	-11.1	-2.6
0 (ZIF-8)	-11.1	-2.5

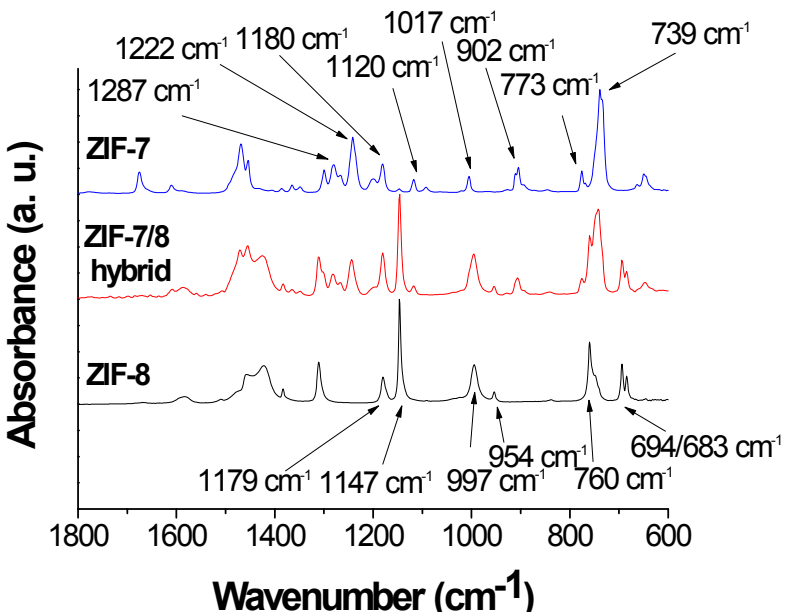

Fig. S8. FTIR spectra of ZIF-7, ZIF-8 and ZIF-7/8 hybrid.

The infrared spectra of ZIF-7, ZIF-8 and the hybrid material are shown in Fig. S8. ZIF-8 shows very intense bands in the 600-1700 cm^{-1} range. In this range ZIF-8 shows signals at 954 and 997 cm^{-1} and two intense bands at 1146 and 1179 cm^{-1}, the latter being attributed to C-N ring vibrations [13,14].In this range, peaks at 683, 694, 760 cm^{-1} are also clearly visible. These are mainly attributed to in-plane C-H deformation bands. [15] [16],[17] In the case of ZIF-7, this framework also shows very intense bands in the 600-1700 cm^{-1} range but different to those of ZIF-8. The absorbance peak at 1017 cm^{-1} is assigned to the benzene-ring vibration and the signal at 1287 cm^{-1} is related to the imidazole-ring breathing. The peak at 1222 cm^{-1} is caused by the in-plane C-H deformation of the disubstituted benzimidazole, while the peak at 902 cm^{-1} is due to the C–H out-of-plane bending of single hydrogen in substituted benzene rings. Finally, the signals at 1180, 1120 and 773 cm^{-1} are due to the benzimidazole in-plane C-H bending, the N-H in-plane bending and the imidazole in-plane ring bending, respectively.[18] The hybrid material spectrum consists of the full combination of all the signals observed in ZIF-7 and ZIF-8 patterns, since all the vibration modes can be seen in it.

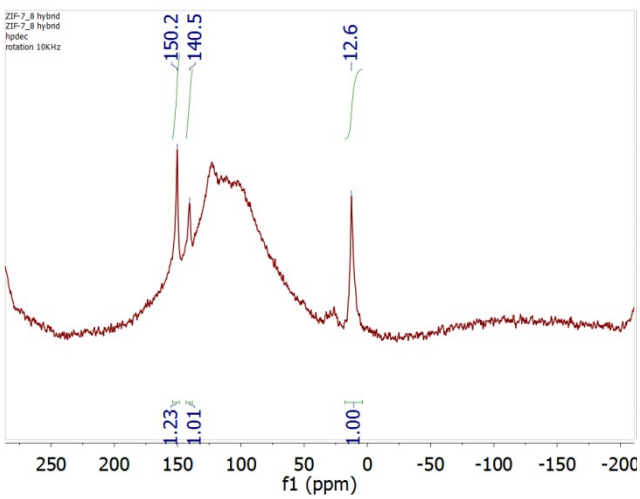

Fig. S9. Quantification of bIm by ^{13}C NMR in ZIF-7/8 (10 %mol bIm) framework.

The amount of bIm in the hybrid ZIF was also calculated with another experiment decoupling the ^{1}H signal in the ^{13}C NMR pattern (see Fig. S9). The resonance at 150.2 ppm corresponds to the contribution of two different carbons, one from mIm (C_{1m}) and another from bIm (C_{1b}). Adjusting the integration area of the peaks whose signal is only due to one carbon atom, thus C_{3m} (12.6 ppm)(mIm) and C_{7b} (140.5 ppm)(bIm) to unit, its integrated area was of 1.23. This means that an 18% of this signal is related to the bIm molecule.

Membrane characterization:

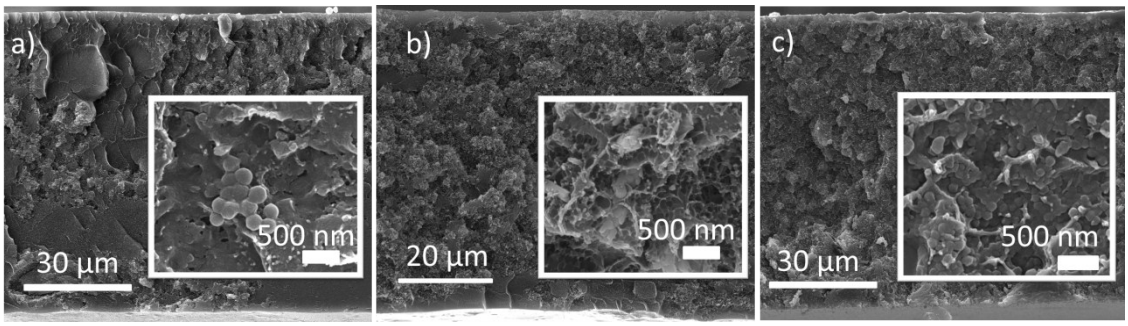

Fig. S10. SEM images of the PBI MMMs containing 10 wt% (a), 20 wt% (b) and 32 wt% (c) of the ZIF-7/8 hybrid (10 wt% mol bIm)

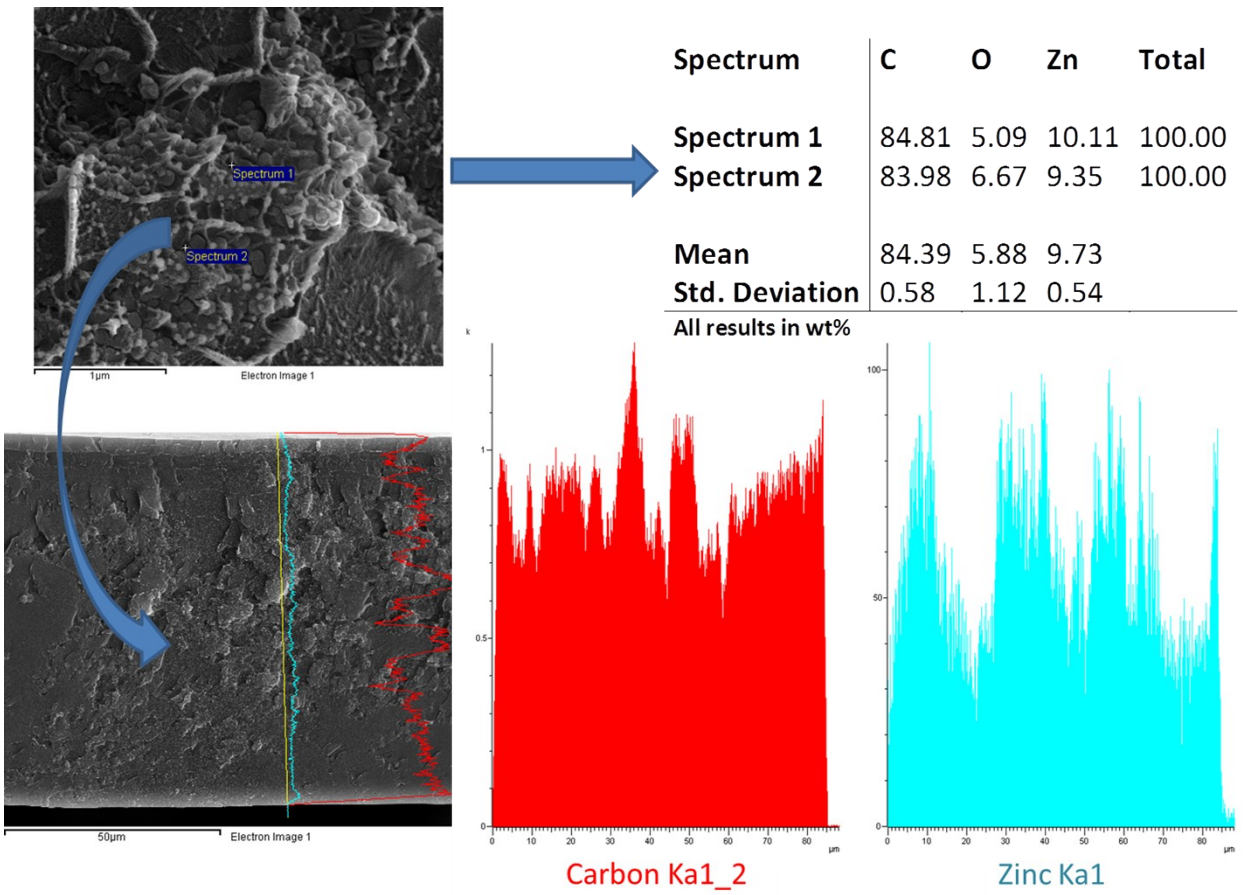

Spectrum	C	O	Zn	Total
Spectrum 1	84.81	5.09	10.11	100.00
Spectrum 2	83.98	6.67	9.35	100.00
Mean	84.39	5.88	9.73	
Std. Deviation	0.58	1.12	0.54	

All results in wt%

Figure S11. SEM-EDX of the cross-section of a 10 wt% loaded hybrid/PBI MMM where can be distinguished C (in red) and Zn (in blue). Weight percentage calculated from the whole section (spectra 1 and 2) are included in the table.

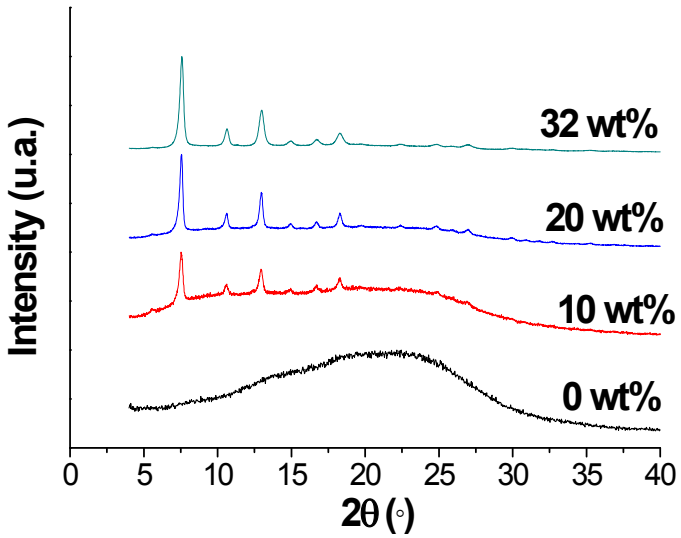

Fig. S12. XRD patterns of the PBI MMMs containing 10 wt% (a), 20 wt% (b) and 32 wt% (c) of the ZIF-7/8 hybrid.

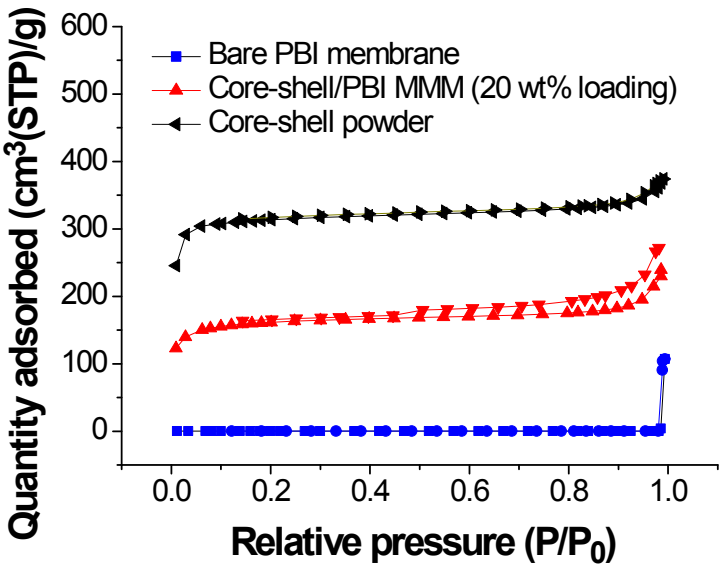

Fig. S13. N_2 adsorption isotherms of bare PBI membrane, 20 wt% ZIF-7/8 hybrid core-shell MMM and activated core-shell (10 mol% bIm) powder. Volume for MMM is related to ZIF7/8 hybrid core-shell mass.

N_2 adsorption was additionally measured for pure PBI and MMM containing 20 wt% loading of ZIF-7/8 hybrid material for comparison with the core-shell powder (shown in Fig. S6). As expected, PBI did not practically adsorb N_2 (BET specific surface area of 0.4 ±0.0 m^2/g) while the ZIF-7/8 core-shell material when embedded in PBI exhibited an intermediate adsorption capacity (BET specific surface area of 549±9.0 m^2/g) when compared to ZIF-7/8 powder (10 mol% of bIm) (BET specific surface area of 1050±19.0 m^2/g).

Membrane performance:

Table S6. Permeation selectivity values of ZIF-7, ZIF-8 and both hybrids at 453 and 523 K.

Structure	T (^{0}C)	Gas	Loading. θ (mol/kg framework)	Self-diffusion.D (10^{-8} m^2s^{-1})	Adsorption selectivity (-)	Diffusion selectivity (-)	Permselectivity (-)
ZIF-8	180	CO_2	0.19	1.59	0.29	4.52	1.31
		H_2	0.06	7.23			
Hybrid (10 % bIm)	180	CO_2	0.21	2.50	0.25	6.92	1.73
		H_2	0.05	17.00			
Hybrid (44% bIm)	180	CO_2	0.22	0.32	0.14	57.79	8.09
		H_2	0.03	18.80			
ZIF-7	180	CO_2	0.47	0.01	0.03	100.67	3.02
		H_2	0.02	0.71			
ZIF-8	250	CO_2	0.12	3.04	0.38	4.00	1.52
		H_2	0.12	3.04			
Hybrid (10 % bIm)	250	CO_2	0.05	12.10	0.34	12.24	4.16
		H_2	0.04	27.80			
Hybrid (44% bIm)	250	CO_2	0.11	0.88	0.26	9.27	2.41
		H_2	0.03	8.08			
ZIF-7	250	CO_2	0.18	0.01	0.07	217.14	15.2
		H_2	0.01	2.10			

Table S6 shows the permeation selectivities of ZIF-7, ZIF-8 and the hybrid ZIFs at 180 and 250^0C. All ZIFs are H_2 selective since their permselectivity values are over the unit. The H_2/CO_2 adsorption selectivities are in the range of 0.07-0.38 while diffusion selectivities show a huge range from 4 to over 200. Diffusion very strongly favors H_2 over CO_2. Noteworthy that the self-diffusion values are the highest for the hybrid material, especially for H_2, explaining how the PBI MMMs containing hybrid material show such high permeabilities, superior to that of MMMs containing neat ZIFs.

1- References

1 N. Liédana, A. Galve, C. Rubio, C. Téllez and J. Coronas, *ACS Appl. Mater. Interfaces,* 2012, **4,** 5016-5021.
2 Y.-S. Li, F.-Y. Liang, H. Bux, A. Feldhoff, W.-S. Yang, J. Caro, *Andgew. Chem. Int. Ed.,* 2010, 548–551.
3 D. Dubbeldam, S. Calero, D. E. Ellis and R. Q. Snurr, *Mol. Simul.,* 2016, **42,** 81-101.
4 J. J. G. Sevillano, S. Calero, C. O. Ania, J. B. Parra, F. Kapteijn, J. Gascon and S. Hamad, *J. Phys. Chem. C,* 2012, **117,** 466-471.
5 A. K. Rappé, C. J. Casewit, K. Colwell, W. Goddard Iii and W. Skiff, *J. Am. Chem. Soc.,* 1992, **114,** 10024-10035.
6 S. L. Mayo, B. D. Olafson and W. A. Goddard, *J. Phys. Chem.,* 1990, **94,** 8897-8909.
7 D. Dubbeldam and R. Snurr, *Mol. Simul.,* 2007, **33,** 305-325.
8 X. Wu, J. Huang, W. Cai and M. Jaroniec, *RSC Advances,* 2014, **4,** 16503-16511.
9 P. Zhao, G. I. Lampronti, G. O. Lloyd, M. T. Wharmby, S. Facq, A. K. Cheetham and S. A. Redfern, *Chem. Mater.,* 2014, **26,** 1767-1769.
10 D. Fairen-Jimenez, S. Moggach, M. Wharmby, P. Wright, S. Parsons and T. Duren, *J. Am. Chem. Soc.,* 2011, **133,** 8900-8902.
11 S. Aguado, G. Bergeret, M. P. Titus, V. Moizan, C. Nieto-Draghi, N. Bats and D. Farrusseng, New *J. Chem.,* 2011, **35,** 546-550.
12 J. van den Bergh, C. Gücüyener, E. A. Pidko, E. J. Hensen, J. Gascon and F. Kapteijn, *Chem. Europ. J.,* 2011, **17,** 8832-8840.
13 Q. Song, S. Nataraj, M. V. Roussenova, J. C. Tan, D. J. Hughes, W. Li, P. Bourgoin, M. A. Alam, A. K. Cheetham and S. A. Al-Muhtaseb, *Energy Environ. Sci.,* 2012, **5,** 8359-8369.
14 G. Kumari, K. Jayaramulu, T. K. Maji and C. Narayana, *J. Phys. Chem. A,* 2013, **117,** 11006-11012.
15 M. Cordes and J. Walter, *Spectrochim. Acta, Pt. A: Mol. Spectrosc.,* 1968, **24,** 1421-1435.
16 P. Musto, F. Karasz and W. MacKnight, *Polymer,* 1993, **34,** 2934-2945.
17 P. Christensen and S. Jones, *Polym. Degrad. Stab.,* 2014, **105,** 211-217.
18 D. P. Drolet, D. M. Manuta, A. J. Lees, A. Katnani and G. J. Coyle, *Inorg. Chim. Acta,* 1988, **146,** 173-180.